

Article

Synthesis of Bimetallic Gold-Silver (Au-Ag) Nanoparticles for the Catalytic Reduction of 4-Nitrophenol to 4-Aminophenol

Nurafaliana Berahim ^{1,2,*} , Wan Jeffrey Basirun ^{2,3}, Bey Fen Leo ^{2,4}  and Mohd Rafie Johan ²

¹ Advanced Materials Research Laboratory, Department of Mechanical Engineering, Faculty of Engineering, University of Malaya, Kuala Lumpur 50603, Malaysia

² Nanotechnology and Catalysis Research Center (NANOCAT), University of Malaya, Kuala Lumpur 50603, Malaysia; jeff@um.edu.my (W.J.B.); beyfenleo@um.edu.my (B.F.L.); mrafiej@um.edu.my (M.R.J.)

³ Department of Chemistry, Faculty of Science, University of Malaya, Kuala Lumpur 50603, Malaysia

⁴ Faculty of Medicine, University of Malaya, Kuala Lumpur 50603, Malaysia

* Correspondence: nurafalianaberahim@um.edu.my; Tel.: +603-7967-6959

Received: 6 August 2018; Accepted: 11 September 2018; Published: 25 September 2018



Abstract: Bimetallic gold-silver nanoparticles as unique catalysts were prepared using seed colloidal techniques. The catalytic capabilities of the nanoparticles were ascertained in the reduction of 4-nitrophenol to 4-aminophenol in the presence of sodium borohydride. Our results clearly showed that the rate of 4-NP reduction to 4-AP increased with a corresponding decrease in the diameter of the bimetallic NPs. The Au-Ag nanoparticles prepared with 5.0 mL Au seed volume indicated higher reduction activity, which was approximately 1.2 times higher than that of 2.0 mL Au seed volume in the reductive conversion of 4-NP to 4-AP. However, the monometallic NPs showed relatively less catalytic activity in the reductive conversion of 4-NP to 4-AP compared to bimetallic Au-Ag nanoparticles. Our studies also reinforced the improved catalytic properties of the bimetallic Au-Ag nanoparticles structure with a direct impact of the size or diameter and relative composition of the bimetallic catalytic nanoparticles.

Keywords: bimetallic; monometallic; gold-silver; catalytic; nitrophenol

1. Introduction

In the recent years, bimetallic nanoparticles (NPs) have received the increased attention of the researchers due to their excellent optical, magnetic, electronic, and catalytic properties compared to their individual analogues [1]. The structure of bimetallic NPs is composed of two different elements that are either present in a core-shell arrangement or exist as randomly dispersed alloys [2]. Bimetallic NPs not only possess the combination properties of both metals but also produce emerging properties due to the synergistic effect between two metals [3]. The literature reported the preparation of different bimetallic NPs combinations, e.g., Au-Ag, Au-Cu, Ag-Au, and Ag-Cu [4–7]. The selected bimetallic NPs such as Au-Ag system were of particular interest compared to their monometallic analogue due to the following reasons: (a) The Au-Ag bimetallic NPs have tunable surface plasmon (SP) bands in the visible range of Au at 520 nm and Ag at 400 nm [8]; (b) The metallic Au and Ag NPs have a similar crystal structure, which is face-centered cubic (FCC), with extremely similar lattice constants values of 0.479 nm and 0.486 nm, respectively [9–11]; (c) The selected metallic NPs possess excellent chemical stability, facile preparative methods, and good catalytic activity towards reduction of the aromatic nitro compounds to amine derivatives [12,13].

Gold nanoparticles (Au NPs) have been widely used in spectroscopy, biomedicine, catalysis, environmental biotechnology, and electrochemistry [14]. Several physical and chemical ways have been developed to prepare Au NPs; however, the Turkevich method, which uses reducing and stabilizing agent and water as solvent, is the most preferable [15]. The advantages of this method can yield monodispersed and dimension range of 7–100 nm Au NPs [16]. Au NPs have attracted more attention due to their high catalytic activities under mild conditions such as in organic reactions [17,18]. This is exemplified by hydrogenation reactions of unsaturated carbonyls and the reduction of nitro groups; alkyne activation; coupling reactions; and oxidation reactions of cyclohexane, toluenes, alcohols, and alkenes [18]. In addition, Au NPs with different shapes synthesized via microwave also have been used as catalysts in the reduction of p-nitroaniline at room temperature [19]. Staykov et al. [20] have studied gold nanoparticles for aerobic oxidation of alkenes, which act as a catalyst to weakly bind the reactants and stabilize the alkyl radicals in the intermediate state between the first and second reaction steps.

The bimetallic NPs offer extraordinary catalytic, magnetic, electronic, and optical properties due to the presence of two metals in their structures, leading to wide range applications such as catalysis, surface-enhanced Raman scattering (SERS), and biosensors [3,21–23]. Holden et al. [22] has found that Ag-Au NPs showed a higher rate of 4-NP reduction compared with monometallic Ag or Au NPs due to greater surface areas of bimetallic Ag-Au NPs. The author also indicated that the catalytic activity was influenced by the electronic effects in which adsorbate binds to Au and Ag surfaces [22]. Chen et al. [24] reported that the catalytic activity of 4-NP reduction using Au-Pd on graphene nanosheets showed a higher rate in comparison with monometallic counterparts due to the synergistic effect of Au and Pd species. There are various methods employed to prepare bimetallic Au-Ag NPs, which include successive reduction, laser ablation, solvent extraction-reduction, microemulsion, galvanic replacement, and colloidal synthesis [25–27]. Colloidal synthesis is one of the most commonly used, because it offers a great variety of options for composition, size, crystal structure, shape, and surface chemistry control due to the flexibility in selecting the reaction system and synthesis condition [26,27]. In addition, this method also takes advantage of surface catalysis [28]. Czaplinska and co-workers stated the preparation procedures of bimetallic NPs can improve their catalytic reduction reaction by tuning the size, structure, composition, and distribution [29]. Fu et al. [30] prepared bimetallic Au-Ag NPs using the co-reduction method and their catalytic properties by monitoring the reduction of 4-nitrophenol.

In chemical industries, 4-nitrophenol (4-NP) is widely utilized to produce pesticides, drugs, and synthetic dyes [31–33]. The conversion of 4-NP to 4-AP can be widely used in manufacturing of many analgesics and antipyretic drugs, such as paracetamol, phenacetin, and so on. From that, there is great industrial demand for aromatic amino compounds [27]. In addition, the model reaction of the reduction of 4-NP to 4-AP is selected, because it can easily monitor the reaction kinetics by UV-Vis spectroscopy during the color changes associated with the conversion of 4-nitrophenolate to 4-aminophenol. The catalytic activities of the nanoparticles were evaluated by two types of catalytic reactions at room temperature. The first reaction studied here is the reduction of 4-NP to 4-AP in the absence of catalyst. The second reaction we studied here is the presence of NaBH₄ and nanocatalysts. Leishangthem et al. [34] have prepared the nanoparticles with diameter size more than 5 nm for the reduction of nitrophenol with less than one hour. Al-Kahtani and coworkers have shown that the Au NPs with the diameters range between 10 and 35 nm for the reduction of 4-NP [35].

In this study, the effect of the different nanoparticles on the 4-nitrophenols reduction in the presence of sodium borohydride was investigated. The reduction of 4-nitrophenols was further studied with different sizes of bimetallic nanoparticles. The preparation of bimetallic Au-Ag NPs using the seed colloidal technique was introduced to control the shape and size of nanoparticles through the temporal separation of the nucleation and growth processes [36]. The pre-formed seeds of one metal act as nucleation sites for the further growth of the second metal NPs [37]. In addition, this method also does not require expensive equipment but can be used to produce nanoparticles in a liquid dispersion, which is the desirable form for many applications [26].

2. Results and Discussions

2.1. UV-Visible Spectroscopic Analysis

Figure 1 shows the absorbance spectra of Au NPs and Au-Ag bimetallic NPs. The as-synthesized Au NPs exhibited a surface plasmon resonance (SPR) band around 523 nm, while Au-Ag bimetallic NPs showed SPR peaks at 450 nm and 435 nm, respectively (see Figure 1a). The maximum absorbance spectra of bimetallic NPs show a single peak, suggesting a homogeneous colloidal mixture of the Au and Ag nanoparticles without signifying formation of independent particles [36,38]. The solution color changes from light pink to yellow-orange with the addition of AgNO_3 and ascorbic acid solution, indicating the deposition of Ag layer onto the surface of Au NPs. The ascorbic acid and citrate solutions serve as a weak reducing agent for the reduction of Ag ions and also as a stabilizing agent [38]. The stabilizing agents prevented the agglomeration of the newly formed nanoparticles. The SPR band gives useful information about the size of the synthesized nanoparticles. This is because the frequency and width of SPR rely on the size of the nanoparticles, as well as on the dielectric constant of the metal itself and the surrounding medium [39]. From the UV-Vis absorbance spectra, it was observed that the SPR band gradually shifted to higher wavelengths region as the seed volume decreased, signifying the formation of bimetallic Au-Ag nanoparticles with relatively larger diameters. The optical properties of the Au-Ag NPs exhibited a plasmon resonance at 450 nm and 435 nm, which corresponded to particles that are mostly in Ag character. Generally, it is known that Ag NPs have plasmon absorbance at about 400 nm [25].

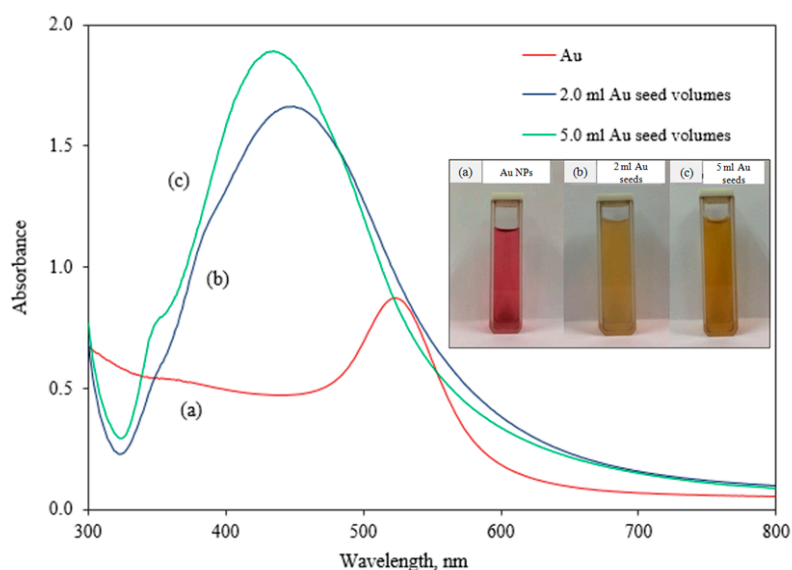


Figure 1. Absorption spectra of (a) Au NPs, and Au-Ag bimetallic NPs with (b) 2.0 mL and (c) 5.0 mL Au seed volumes.

2.2. Transmission Electron Microscopy (TEM) and Energy Dispersive X-Ray Spectroscopy (EDS) Analysis

Figure 2 shows the TEM images and particle size distribution of Au and Au-Ag NPs. The mean diameter of Au NPs was around 24.1 ± 2.7 nm. Figure 2a indicated that the Au NPs were monodispersed with a spherical shape, while Figure 2b,c demonstrated the TEM images of bimetallic Au-Ag NPs at different volume of Au seeds. TEM images of the NPs revealed that most of the bimetallic Au-Ag NPs were approximately spherical in shape and well dispersed. The mean diameter of the bimetallic Au-Ag NPs was approximately 75.2 ± 5.3 nm and 55.2 ± 6.0 nm, corresponding to 2.0 mL and 5.0 mL of Au seed, respectively. The mean diameter of bimetallic Au-Ag NPs is larger than pure Au NPs, indicating that the gold nanoparticles are mixed by silver [38]. The TEM is a well-known method to confirm the bimetallic structures of nanoparticles between gold and silver due

to the contrast difference caused by the atomic number Z of gold and silver (79 for Au; 47 for Ag) [40]. From the mean diameter values of Au-Ag NPs, the particle size is 2.0 mL Au seed was larger than the 5.0 mL Au seed, which is consistent with the UV-vis results.

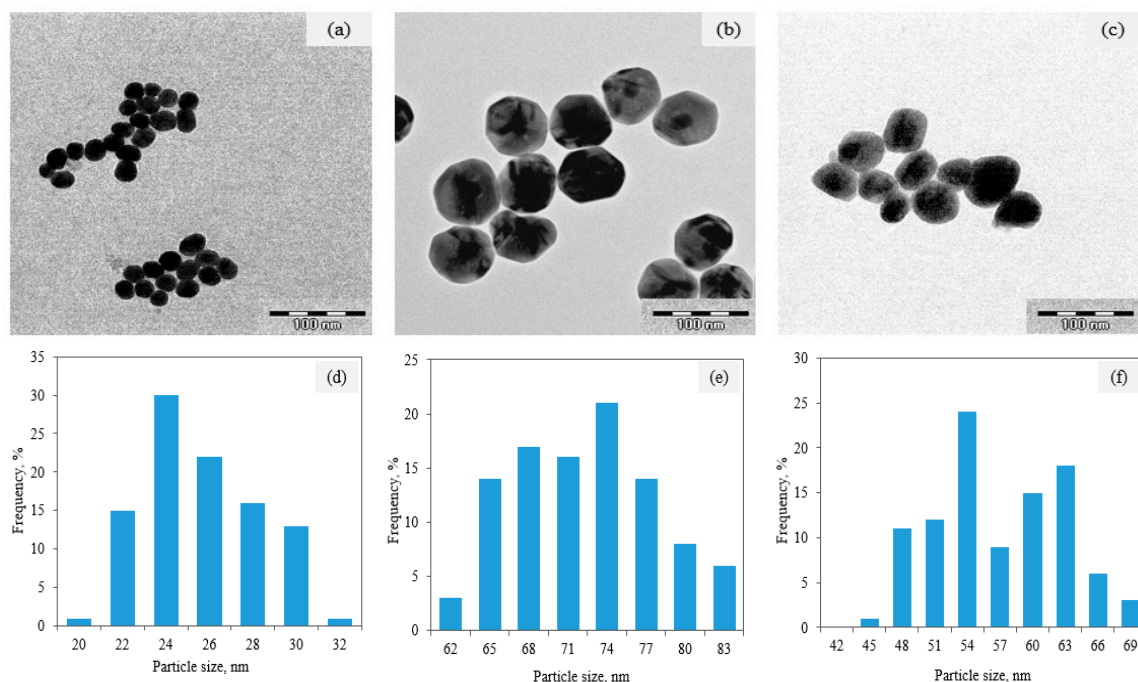


Figure 2. TEM images and corresponding particle size distribution of Au NPs (a,d), Au-Ag bimetallic NPs with 2.0 mL Au seeds (b,e), and Au-Ag NPs with 5.0 mL Au seeds (c,f).

The EDS spectra of Au and bimetallic Au-Ag NPs were shown in Figure 3. Figure 3a confirm the presence of Au in the solution. The EDS spectra of Au-Ag NPs with different volumes of Au seeds that are depicted in Figure 3b,c show the presence of Au, Ag, C, and Cu elements. The spectrum of 2.0 mL Au seeds shows peaks corresponding to Au at 2.0, 9.5, and 11.5 keV, while the peak at 3.2 keV was attributed to Ag. Meanwhile, 5.0 mL of Au NPs seed spectrum shows Au and Ag peaks at 2.0 and 3.0 keV, respectively. The EDS results confirmed the presence of Au and Ag elements in the bimetallic NPs. However, the presence of carbon and copper peaks in the spectrum was due to the copper grid.

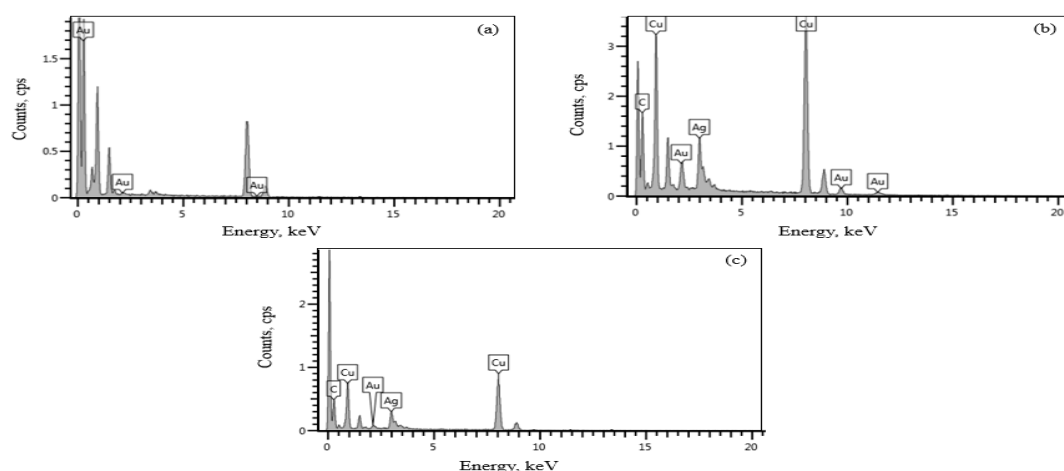


Figure 3. EDS spectra of (a) Au NPs, and Au-Ag bimetallic NPs at different volumes of (b) 2.0 mL and (c) 5.0 mL Au seeds.

2.3. X-ray Diffraction (XRD) Analysis

Figure 4 demonstrates the XRD patterns of Au NPs and bimetallic Au-Ag NPs at different volumes of Au seed. Au NPs show four diffraction peaks (Figure 4a) at the angle of 2θ of 38.1° , 44.5° , 64.7° , and 77.7° , corresponding to (111), (200), (220), and (311) planes, respectively. This is a face-centered cubic (FCC) gold lattice [41,42]. The XRD pattern of bimetallic Au-Ag NPs for 2.0 mL Au seed shows peaks at (111), (200), (220), and (311) planes, respectively, for $2\theta = 38.05^\circ$, 44.30° , 64.50° , and 77.34° . Meanwhile, the XRD pattern of Au-Ag NPs for 5.0 mL Au seed shows intense peaks at angle of 38.12° , 44.40° , 64.17° , and 77.38° corresponding to (111), (200), (220), and (311) planes, respectively [12]. The monometallic Au NPs and bimetallic Au-Ag NPs have the same XRD patterns, because gold and silver have similar lattice constants [9–11].

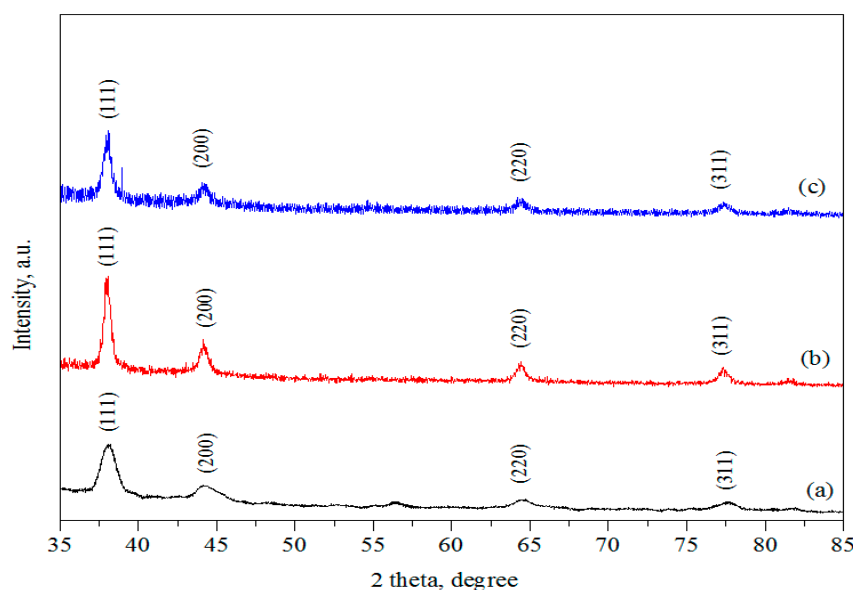


Figure 4. XRD patterns of the (a) Au NPs, and Au-Ag bimetallic NPs at (b) 2.0 mL and (c) 5.0 mL Au seed volumes of Au seed.

2.4. High-Resolution Electron Microscopy (HRTEM) Analysis

Figure 5a–c illustrates the HRTEM images of the Au-Ag bimetallic NPs. A significant change in the contrast between the dark and lighter region indicated the formation of the bimetallic Au-Ag NPs. Figure 5c shows a 0.20 nm lattice spacing, which was indexed to the (200) plane of face-centered cubic (FCC) of silver [42], whereas the measured lattice spacing of 0.23 nm matched well with the (111) planes of FCC gold [9,43].

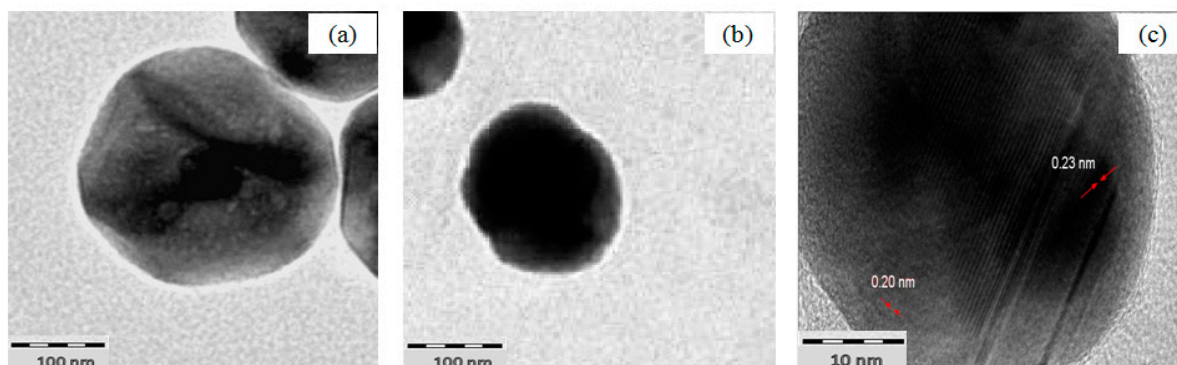


Figure 5. HRTEM images of Au-Ag bimetallic NPs for different volume of Au seed (a) 2.0 mL and (b) 5.0 mL, and (c) lattice spacing of Au-Ag NPs.

2.5. High-Angle Annular Dark-Field Scanning Transmission Electron Microscopy (HAADF-STEM) Analysis

The HAADF-STEM images of the bimetallic Au-Ag NPs obtained in Figure 6a,e showing a contrast between Au and Ag elements, which are dominated by Rutherford scattering [44]. Since the signal in HAADF-STEM mode depends on the atomic number of the elements, the strong brightness corresponding to the Au (heavy element) and the low brightness refer to the Ag (lighter element). The image clearly shows the distribution of the Au and Ag elements in the bimetallic nanoparticles. The EDS elemental mapping analysis boxed in HAADF-STEM in Figure 6b,f were done to confirm their structure and Au and Ag chemical composition. According to the EDS mapping as shown in Figure 6c,d,g,h, the presence of Au signal (yellow) and Ag signal (turquoise) in the bimetallic nanoparticles was indicated.

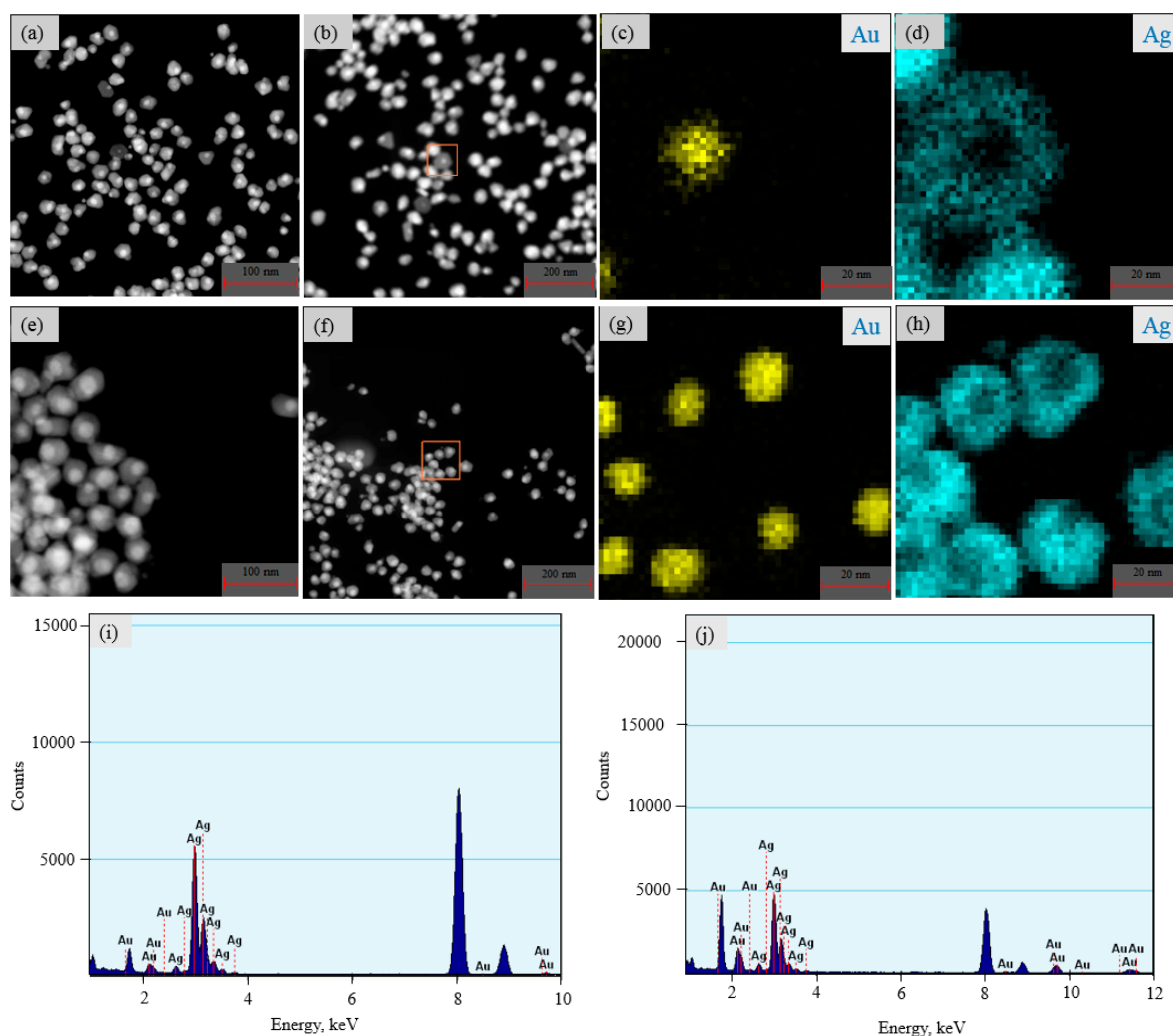


Figure 6. HAADF-STEM images of (a,b) 2.0 mL Au seeds, (e,f) 5.0 mL Au seeds, EDS mapping analysis (c,d,i) 2.0 mL Au seeds, and (g,h,j) 5.0 mL Au seeds of Au-Ag nanoparticles.

2.6. Zeta Potential Analysis

The zeta potential values of Au NPs and bimetallic Au-Ag NPs of different volumes of Au seed were represented in Table 1. The zeta potential of Au NPs relies on the surface modification of the nanoparticles [43]. The Au NPs zeta potential has a negative value of -39.2 mV due to the charge stabilization through the electrostatic interaction between the Au NPs and citrate ions [45]. Meanwhile, the zeta potentials of the bimetallic Au-Ag NPs were -31.5 mV and -20.9 mV for 2.0 mL and 5.0 mL Au seed, respectively. The negative zeta potential value revealed that the Au NPs and bimetallic

Au-Ag NPs possess moderate stability [46]. These values are associated with the stability of the nanoparticles, which could be related to the agglomeration phenomenon. In addition, there is less agglomeration at higher zeta potential values, which causes the nanoparticles to grow larger. The aggregation in aqueous solution is due to the surface hydrophobicity, which causes eventual loss of catalytic activity [47]. In this case, sodium citrate was used to prevent the particle aggregation during the synthesis process of nanoparticles.

Table 1. Particle size and zeta potential for Au NPs and bimetallic Au-Ag NPs.

Sample	Particle Size (nm)	Zeta Potential (mV)
Au NPs	24.1 ± 2.7	−39.2
Au-Ag NPs (2.0 mL Au seed)	75.2 ± 5.3	−31.5
Au-Ag NPs (5.0 mL Au seed)	55.2 ± 6.0	−20.9

2.7. Catalytic Activity of 4-NP Reduction

Figure 7a,b illustrates the catalytic reactions with the 4-NP. The reaction mechanism can be explained by the inherent hydrogen adsorption by Au NPs that transported the hydrogen between NaBH_4 and 4-NP. The hydrogen that comes from the NaBH_4 reduces water. In brief, this behaviour may be explained by the fact that Au NPs adsorb hydrogen from NaBH_4 and efficiently release it during the reduction reaction. Hence, Au NPs act as a hydrogen carrier in this reduction reaction [39]. In a neutral or acidic medium, the 4-NP solution showed a strong absorption peak at 317 nm (Figure 8) [32,33,48]. The addition of NaBH_4 deprotonated the OH group of 4-NP and formed 4-nitrophenolate ion appearing at 400 nm in the UV-vis spectrum [49]. The color of the 4-NP solution changed from light yellow to bright yellow immediately due to the 4-nitrophenolate ion formation [33,42]. The reduction of 4-NP does not occur without the presence of a catalyst [46,48]. The thermodynamically favorable reduction of 4-NP to 4-AP ($E_0 = -0.76$ V vs. NHE) and $\text{H}_3\text{BO}_3/\text{BH}_4^-$ ($E_0 = -1.33$ V vs. NHE) produced large potential difference with negative free energy. The normal hydrogen electrode (NHE) is a reference electrode and includes the solvation process of the proton [50]. However, the presence of a large energy between the mutually repelling negative ions of 4-NP and BH_4^- was responsible for the slow kinetics of the reaction [31,48]. Alternatively, an introduction to Au-Ag NPs can absorb negative ions and able to act as electronic relay systems to transfer electrons donated by borohydride ions to the nitro groups of 4-NP, which is expected to lower the kinetic barrier and thus catalyze the reduction [24].

Metallic nanoparticles are known to catalyze the reduction reaction by facilitating the electron transfer process from the donor BH_4^- to the 4-NP acceptor [49]. With the addition of 0.2 mL catalyst to the reaction mixture containing 3 mL 4-NP and 0.5 mL NaBH_4 , the absorption peak at 400 nm gradually decreased with the passage of time with the simultaneous appearance of a new peak at 300 nm attributed to the 4-AP formation [48]. The UV-vis spectra also showed an isosbestic point at 317 nm, indicating the reduction of 4-NP to 4-AP without any by-product formation [51]. The progress of the reduction reactions was monitored by measuring the absorption spectrum of 4-NP and 4-AP as a function of time by applying different catalysts such as Au and Au-Ag NPs. In the control reduction experiments, only a slight change in the absorption intensity was observed at 400 nm for 4-NP in the absence of a catalyst after 11 min, as shown in Figure 9a. The spectra indicated that the 4-NP was not reduced by the NaBH_4 , and the mixture remained yellow [42]. In contrast, when Au and Au-Ag nanoparticles were used as the catalysts, the absorption intensity at 400 nm decreased, and a new peak appeared at 300 nm attributed to the 4-AP formation [33,42]. The reduction reaction was also visible through color change with bleaching of the color yellow, indicating complete reduction of 4-NP [51].

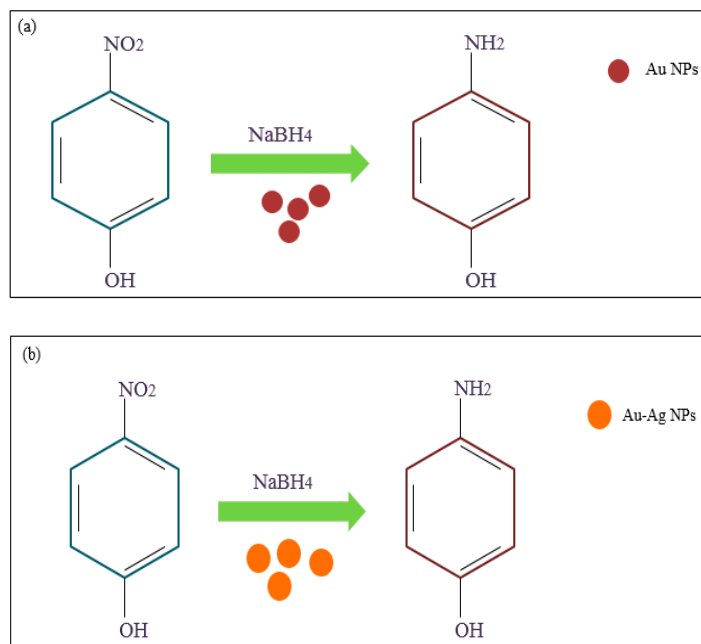


Figure 7. Schematic illustration of the catalytic experiments of 4-NP with (a) Au NPs and (b) Au-Ag NPs.

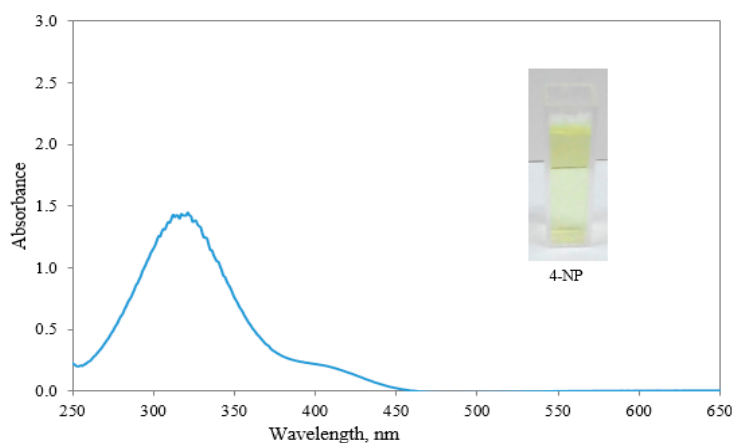


Figure 8. Absorption spectra of 4-NP without reducing agent.

It was noted that the reduction reaction rate of bimetallic Au-Ag NPs was faster compared to monometallic Au NPs. Haldar et al. [49] reported that the catalytic activity of Au-Ag bimetallic NPs is much higher than that associated with the pure Au NPs. These results can be explained by the following factors. First, the improved reduction rates were ascribed to the synergistic effect between the Au and the Ag [42]. Electrons could transfer from Ag to Au owing to the synergistic effect that produced, leading to an increase in the electron density on the surface of the bimetallic Au-Ag NPs, which improved the catalytic activity [52]. Second, the structure could effect the interactions between the two metals [52]. The comparison between two types of bimetallic nanoparticles (2.0 and 5.0 mL Au seeds volumes) reduction rates indicated the practical role of the size and composition effect, as it influenced the time needed for the completion of the reduction reaction. Holden et al. [22] also stated that the catalytic properties of bimetallic nanoparticles can be influenced by their size and composition. The present role of the particle size may also due to the change in the surface area of the smaller size NPs compared to the bulky sized NPs. It is well-known fact that the surface area increases with a corresponding decrease in the NPs particle sizes [36,48]. The increased surface area of the smaller sized NPs contributed to the excellent catalytic activity [36,48]. The surface area of 5.0 mL Au seed volume of Au-Ag NPs was 1.3 times higher compared

to the 2.0 mL Au seed volume Au-Ag NPs [49]. The improved surface area was the reason behind the improved catalytic performance of the 5.0 mL Au seed volume of Au-Ag NPs. The reduction reaction completed in 5 min and 8 min for the 5.0 mL and 2.0 mL Au seed volumes of the Au-Ag NPs, respectively, as shown in Figure 9g,e, respectively. Table 2 shows the rate constants of the reduction 4-NP using Au and Ag-based catalysts reported previously, which might be the result of different structure, size, and composition. It can see clearly that the reduction of 4-NP can be influenced by the structure, size, and composition of nanoparticles.

The catalytic performance of catalysts highly depends on shape of this catalyst. This is due to the different coordination numbers of atoms on surface. For catalyst with a face-centered cubic (FCC) lattice, the coordination number of atoms on (111), (100), and (110) surfaces is 9, 8, and 7, respectively. The corresponding surface energy was in the order of (111) < (100) < (110), which is the reason why (110) usually exhibited better activity than the other two facets [53,54]. As shown XRD result in Figure 4, the structure of NPs was FCC structure, which is good for catalytic reduction of 4-NP. Difference in shape can be produced with different parameters such as concentration of metal ions, pH, and nature of stabilizing and reducing agents [55]. Regarding the TEM images in Figure 2, the nanoparticles were spherical and were able to reduce the 4-NP to 4-AP with less than 15 min. Gupta et al. [19] have prepared different shapes of Au NPs for catalytic reduction of aromatic nitro compounds, and their results show that spherical Au NPs are the second-best catalyst compared to cubes, polyhedral, and tetrahedral shapes. In addition, there is no significant difference in reduction time between the spherical and cubic shapes, which is about a one-minute difference. In this work, bimetallic, spherical Au-Ag NPs have good catalytic activity in the conversion of 4-NP to 4-AP. Based on previous research, the spherical shape of bimetallic Au-Ag NPs can reduce 4-NP faster at room temperature [30].

Table 2. Comparison of the catalytic reduction of 4-NP by Au and Ag catalysts.

Catalysts	Reducing Agents	Rate Constant (min ⁻¹)	Time (min)	Particle Size (nm)	References
Au NPs	NaBH ₄	0.36	14	24.1	This work
Au-Ag bimetallic NPs (2.0 mL Au seed)	NaBH ₄	0.52	8	75.2	This work
Au-Ag bimetallic NPs (5.0 mL Au seed)	NaBH ₄	0.62	5	55.2	This work
Ag dendrite-based Au-Ag nanostructure	NaBH ₄	0.00010	8	-	[23]
Ag/GO NPs	NaBH ₄	0.208	25	7.5	[56]
Au/GO NPs	NaBH ₄	0.368	10	5.0	[56]
Au-Ag/GO alloy NPs	NaBH ₄	0.761	5	6.0	[56]

The concentration of BH₄⁻ used in the system was much higher than the 4-NP, so it was reasonable to assume that the concentration of borohydride ions was constant throughout the reduction reaction. A pseudo first-order kinetics fits the catalytic reduction rate [32,33,42,48]. A linear correlation of ln(A₀/A_t) with time was observed, in which A_t and A₀ was the absorbance at specific intervals and the initial absorbance of 4-nitrophenolate ion, respectively [32,33,42,49]. The rate constants for each system were measured from the slope of the ln(A₀/A_t) vs. time graph, as shown in Figure 9b,d,f,h. The values of the chemical reduction rates were calculated to be 0.02, 0.36, 0.52, and 0.62 min⁻¹ for NaBH₄, Au, 2.0 mL, and 5.0 mL Au seed volume Au-Ag NPs, respectively, as summarized in Table 2. Among all the catalysts, the 5.0 mL Au seed volume Au-Ag NPs catalyst demonstrated the fastest reduction rate, thus resulting in higher catalytic activity for the reduction of 4-NP at room temperature. These experimental phenomena demonstrated that the bimetallic Au-Ag NPs had better catalytic activity for the reduction of 4-NP.

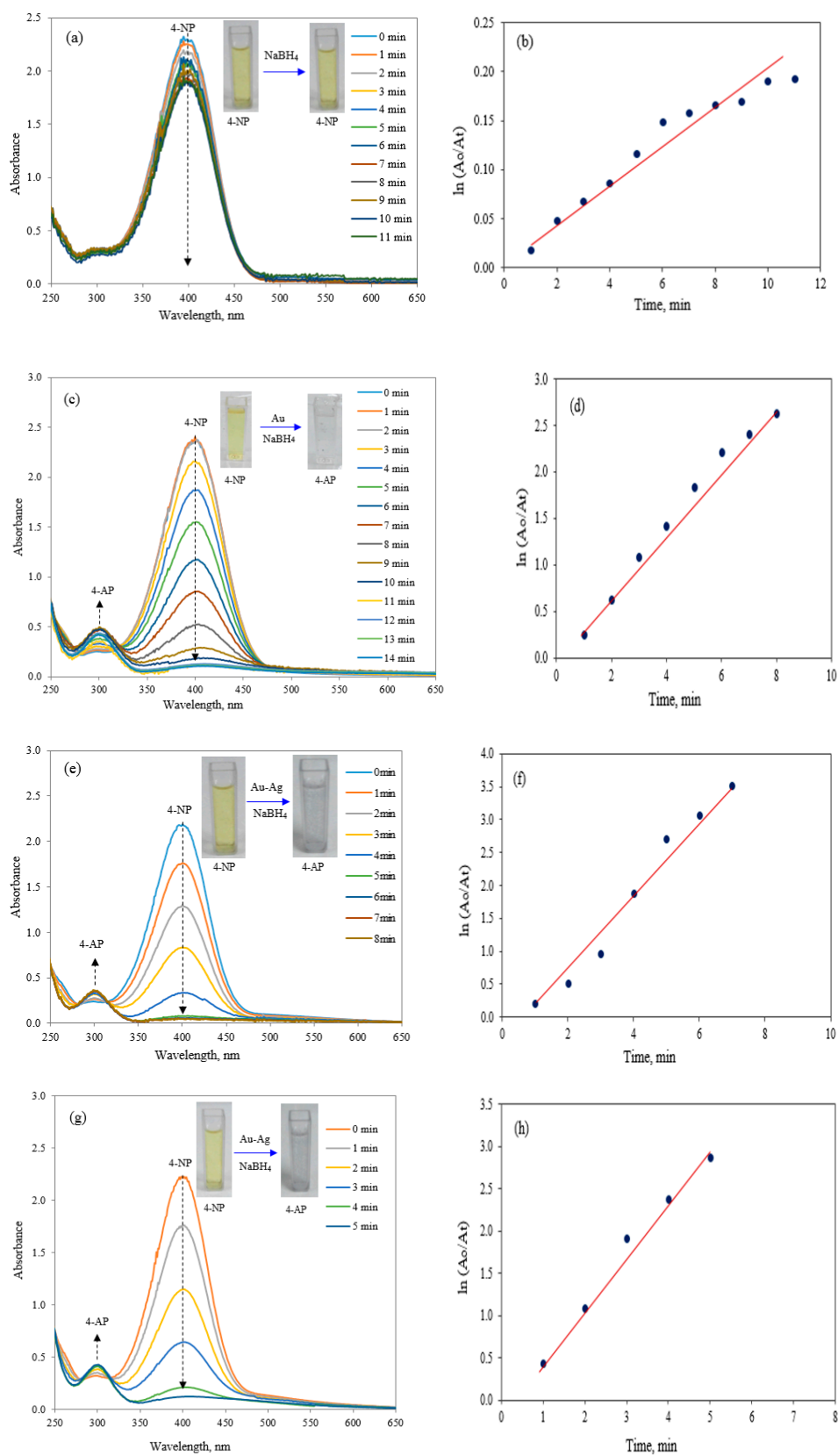


Figure 9. Absorption spectra of 4-NP reduced by (a) NaBH_4 only. NaBH_4 in the presence of (c) Au NPs, (e) 2.0 mL Au seeds volume of Au-Ag NPs, and (g) 5.0 mL Au seeds volume of Au-Ag NPs and corresponding $\ln(A_0/A_t)$ versus time plot for the determination of rate constants for (b) NaBH_4 , (d) Au NPs, (f) 2.0 mL Au seeds volume Au-Ag NPs, and (h) 5.0 mL Au seeds volume Au-Ag NPs.

3. Experimental

3.1. Synthesis of Gold Nanoparticles (Au NPs)

The citrate thermal reduction technique was used for the preparation of colloidal Au NPs [57]. Briefly, an aqueous solution of $\text{HAuCl}_4 \cdot 3\text{H}_2\text{O}$ (Sigma-Aldrich, St. Louis, MO, USA) (1 mL of 1 wt. %) was added to 90 mL of distilled water. The above solution was stirred vigorously along with heating until the boiling point at 100 °C. 2 mL of 38.8 mM of sodium citrate (Sigma-Aldrich, St. Louis, MO, USA) was added dropwise as the reducing and stabilizing agents to prevent the particles aggregation during the synthesis process. The successive color changes from light yellow to maroon upon the addition of sodium citrate. The final solution was left in an ice bath to obtain the uniform size of Au NPs. The as-synthesized NPs solution was washed three times to remove impurities before diluting in deionized water to get desired concentration.

3.2. Synthesis of Bimetallic Gold-Silver Nanoparticles (Au-Ag NPs)

The Au-Ag NPs were prepared using the seed colloidal technique [38]. The as-synthesized citrate-capped Au NPs were used as the seed in the formation of the bimetallic Au-Ag NPs. The different volume of Au NPs (2.0 and 5.0 mL) and 1 mL of sodium citrate solution (38.8 mM) were added to 30 mL of distilled water and stirred for 10 min. Then, 1.2 mL of silver nitrate aqueous solution (10 mM) and 0.4 mL of ascorbic aqueous solution (100 mM) were added dropwise to the above mixture. The reaction mixture was stirred continuously for 30 min to ensure a homogeneous solution at room temperature. The solution was then washed three times and dispersed in deionized water.

3.3. Catalytic Reduction Activity of the Bimetallic Au-Ag NPs

The catalytic activity of the Au-Ag NPs was evaluated by the reductive conversion of 4-nitrophenol to 4-aminophenol. The chemical reduction was carried out in a quartz cuvette containing 3.0 mL of 4-nitrophenol (0.2 mM) and 1.0 mL of distilled water. The addition of aqueous NaBH_4 (0.5 mL, 0.4 M) solution resulted in a color change from light yellow to bright yellow. Finally, 0.2 mL of the Au-Ag NPs was added. The absorbance spectra were recorded at a time interval of 1 min in the wavelength range of 200–800 nm at room temperature.

3.4. Characterizations

The UV-visible measurements were carried out using a CARY 50 UV-vis spectrophotometer (Agilent Technologies, Palo Alto, CA, USA) with centrifuged samples. The HRTEM was performed by TECNAI TF20 X-Twin (FEI, Hillsboro, OR, USA) at an accelerating voltage of 200 kV. High-angle annular dark-field scanning transmission electron microscopy (HAADF-STEM, FEI, Hillsboro, OR, USA) imaging and energy dispersive spectroscopy (EDS, FEI, Hillsboro, OR, USA) elemental mapping were carried out using TECNAI TF20 X-Twin (FEI, Hillsboro, OR, USA) operating at 200 kV to reveal the structure and elemental distributions of Au and Ag in Au-Ag NPs. The samples were pre-sonicated for 10 min to disperse the particles and avoid agglomeration. The sample was dropped on a copper grid and dried in a vacuum desiccator. The TEM (Carl ZEISS, Jena, Germany) images particle size distribution of each sample was measured using *image-J* software. The TEM analysis was used to provide information on the size and morphology of the Au NPs and Au-Ag bimetallic NPs. The EDS analysis was carried out to investigate the composition of the gold and bimetallic gold-silver NPs.

The XRD (PANalytical B.V., Almelo, The Netherlands) measurement of gold and gold-silver NPs was performed using an Empyrean (PANalytical) X-ray diffractometer with a $\text{Cu K}\alpha$ ($\lambda = 1.54 \text{ \AA}$) source. The XRD samples were prepared by drop coating the solution on a glass slide followed by drying at room temperature. The zeta potential analysis was accomplished using Zetasizer Nanoseries ZS (Malvern Instrument Ltd., Malvern, UK) instrument at room temperature to measure the potential stability and surface charge of the nanoparticles [46]. Then, samples were injected into a

disposable capillary cell and inserted into the instrument with an equilibrated sensor to measure the zeta potential values.

4. Conclusions

In the present study, we have successfully employed a seeding-growth technique for the preparation of bimetallic Au-Ag NPs catalysts. It was found that the size or diameter of the bimetallic NPs influenced the catalytic properties of the Au-Ag NPs. The reduction reaction rate for the smaller size (5.0 mL Au seed) of Au-Ag NPs catalysts was higher than the larger size (2.0 mL Au seed) of particles. The bimetallic Au-Ag NPs synergistically improve the catalytic activity compared to the monometallic Au NPs. The study revealed that the catalytic performance on the reduction of 4-nitrophenol was remarkably improved by controlling the size, diameter, and composition of the bimetallic NPs.

Author Contributions: N.B. performed and analysed experiments and wrote the paper; W.J.B., B.F.L., and M.R.J. edited the paper and engaged in the conceptualization, funding, and supervision.

Acknowledgments: We gratefully acknowledge the Center for Research Grant Management (PPGP) of University Malaya for awarding this particular research; a Postgraduate Research Grant (PPP) (PG040-2016A); and the use of facilities funded by grant number (FP039-2016), (GC001C-14SBS), and RU2017.

Conflicts of Interest: The authors declare no conflict of interest.

References

1. Guha, S.; Roy, S.; Banerjee, A. Fluorescent Au@Ag core-shell nanoparticles with controlled shell thickness and Hg^{II} sensing. *Langmuir* **2011**, *27*, 13198–13205. [[CrossRef](#)] [[PubMed](#)]
2. Sanyal, U.; Davis, D.T.; Jagirdar, B.R. Bimetallic core-shell nanocomposites using weak reducing agent and their transformation to alloy nanostructures. *Dalton Trans.* **2013**, *42*, 7147–7157. [[CrossRef](#)] [[PubMed](#)]
3. Zaleska-Medynska, A.; Marchelek, M.; Diak, M.; Grabowska, E. Noble metal-based bimetallic nanoparticles: The effect of the structure on the optical, catalytic and photocatalytic properties. *Adv. Colloid Interface Sci.* **2016**, *229*, 80–107. [[CrossRef](#)] [[PubMed](#)]
4. Yuan, P.; Ma, R.; Gao, N.; Garai, M.; Xu, Q.H. Plasmon coupling-enhanced two-photon photoluminescence of Au@Ag core-shell nanoparticles and applications in the nuclease assay. *Nanoscale* **2015**, *7*, 10233–10239. [[CrossRef](#)] [[PubMed](#)]
5. Hsia, C.F.; Madasu, M.; Huang, M.H. Aqueous phase synthesis of Au-Cu core-shell nanocubes and octahedra with tunable sizes and noncentrally located cores. *Chem. Mater.* **2016**, *28*, 3073–3079. [[CrossRef](#)]
6. Tsuji, M.; Hikino, S.; Tanabe, R.; Yamaguchi, D. Synthesis of Ag@Cu core-shell nanoparticles in high yield using a polyol method. *Chem. Lett.* **2010**, *39*, 334–336. [[CrossRef](#)]
7. Cao, Y.; Jin, R.; Mirkin, C.A. DNA-modified core-shell Ag/Au nanoparticles. *J. Am. Chem. Soc.* **2001**, *123*, 7961–7962. [[CrossRef](#)] [[PubMed](#)]
8. Shen, D.S.; Mathew, J.; Philip, D. Phytosynthesis of Au, Ag and Au-Ag bimetallic nanoparticles using aqueous extract and dried leaf of *Anacardium occidentale*. *Spectrochim. Acta Part A* **2011**, *79*, 254–262. [[CrossRef](#)] [[PubMed](#)]
9. Monga, A.; Pal, B. Improved catalytic activity and surface electro-kinetics of bimetallic Au-Ag core-shell nanocomposites. *New J. Chem.* **2015**, *39*, 304–313. [[CrossRef](#)]
10. Zeng, J.; Cao, Y.; Lu, C.H.; Wang, X.D.; Wang, Q.; Wen, C.Y.; Qu, J.B.; Yuan, C.; Yan, Z.F.; Chen, X. A colorimetric assay for measuring iodide using Au@Ag core-shell nanoparticles coupled with Cu²⁺. *Anal. Chim. Acta* **2015**, *891*, 269–276. [[CrossRef](#)] [[PubMed](#)]
11. Rodríguez-González, B.; Burrows, A.; Watanabe, M.; Kiely, C.J.; Marzán, L.M.L. Multishell bimetallic AuAg nanoparticles: Synthesis, structure and optical properties. *J. Mater. Chem.* **2005**, *15*, 1755–1759. [[CrossRef](#)]
12. Liu, Y.; Zhou, J.; Wang, B.; Jiang, T.; Ho, H.P.; Petti, L.; Mormile, P. Au@Ag core-shell nanocubes: Epitaxial growth synthesis and surface-enhanced Raman scattering performance. *Phys. Chem. Chem. Phys.* **2015**, *17*, 6819–6826. [[CrossRef](#)] [[PubMed](#)]

13. Rather, J.A.; Khudaish, E.A.; Munam, A.; Qurashi, A.; Kannan, P. Electrochemically reduced fullerene–graphene oxide interface for swift detection of Parkinsons disease biomarkers. *Sens. Actuators B* **2016**, *237*, 672–684. [[CrossRef](#)]
14. Li, F.; Li, Z.; Zeng, C.; Hu, Y. Laccase-assisted rapid synthesis of colloidal gold nanoparticles for the catalytic reduction of 4-nitrophenol. *J. Braz. Chem. Soc.* **2017**, *28*, 960–966. [[CrossRef](#)]
15. Bogireddy, N.K.R.; Pal, U.; Gomez, L.M.; Agarwal, V. Size controlled green synthesis of gold nanoparticles using *Coffea arabica* seed extract and their catalytic performance in 4-nitrophenol reduction. *RSC Adv.* **2018**, *8*, 24819–24826. [[CrossRef](#)]
16. Teimouri, M.; Khosravi-Nejad, F.; Attar, F.; Saboury, A.A.; Kostova, I.; Benelli, G.; Falahati, M. Gold nanoparticles fabrication by plant extracts: Synthesis, characterization, degradation of 4-nitrophenol from industrial wastewater, and insecticidal activity—A review. *J. Clean. Prod.* **2018**, *184*, 740–753. [[CrossRef](#)]
17. Shen, W.; Qu, Y.; Pei, X.; Li, S.; You, S.; Wang, J.; Zhang, Z.; Zhou, J. Catalytic reduction of 4-nitrophenol using gold nanoparticles biosynthesized by cell-free extracts of *Aspergillus* sp. WL-Au. *J. Hazard. Mater.* **2017**, *321*, 299–306. [[CrossRef](#)] [[PubMed](#)]
18. Seo, Y.S.; Ahn, E.Y.; Park, J.; Kim, T.Y.; Hong, J.E.; Kim, K.; Park, Y.; Park, Y. Catalytic reduction of 4-nitrophenol with gold nanoparticles synthesized by caffeic acid. *Nanoscale Res. Lett.* **2017**, *12*. [[CrossRef](#)] [[PubMed](#)]
19. Gupta, S.S.R.; Kantam, M.L.; Bhanage, B.M. Shape-selective synthesis of gold nanoparticles and their catalytic activity towards reduction of p-nitroaniline. *Nano-Struct. Nano-Objects* **2018**, *14*, 125–130. [[CrossRef](#)]
20. Staykov, A.; Miwa, T.; Yoshizawa, K. Aerobic oxidation of alkanes on icosahedron gold nanoparticle Au 55. *J. Catal.* **2018**, *364*, 141–153. [[CrossRef](#)]
21. Feng, L.; Gao, G.; Huang, P.; Wang, K.; Wang, X.; Luo, T.; Zhang, C. Optical properties and catalytic activity of bimetallic gold-silver nanoparticles. *Nano Biomed. Eng.* **2010**, *2*, 258–267. [[CrossRef](#)]
22. Holden, M.S.; Nick, K.E.; Hall, M.; Milligan, J.R.; Chen, Q.; Perry, C.C. Synthesis and catalytic activity of pluronic stabilized silver-gold bimetallic nanoparticles. *RSC Adv.* **2014**, *4*, 52279–52288. [[CrossRef](#)] [[PubMed](#)]
23. Huang, J.; Vongehr, S.; Tang, S.; Lu, H.; Shen, J.; Meng, X. Ag dendrite-based Au/Ag bimetallic nanostructures with strongly enhanced catalytic activity. *Langmuir* **2009**, *25*, 11890–11896. [[CrossRef](#)] [[PubMed](#)]
24. Chen, X.; Cai, Z.; Chen, X.; Oyama, M. AuPd bimetallic nanoparticles decorated on graphene nanosheets: Their green synthesis, growth mechanism and high catalytic ability in 4-nitrophenol reduction. *J. Mater. Chem. A* **2014**, *2*, 5668–5674. [[CrossRef](#)]
25. Chen, D.H.; Chen, C.J. Formation and characterization of Au-Ag bimetallic nanoparticles in water-in-oil microemulsions. *J. Mater. Chem.* **2002**, *12*, 1557–1562. [[CrossRef](#)]
26. Zhang, Q.; Xie, J.; Yu, Y.; Lee, J.Y. Monodispersity control in the synthesis of monometallic and bimetallic quasi-spherical gold and silver nanoparticles. *Nanoscale* **2012**, *2*, 1962–1975. [[CrossRef](#)] [[PubMed](#)]
27. Arora, N.; Mehta, A.; Mishra, A.; Basu, S. 4-Nitrophenol reduction catalysed by Au-Ag bimetallic nanoparticles supported on LDH: Homogeneous vs. heterogeneous catalysis. *Appl. Clay Sci.* **2018**, *151*, 1–9. [[CrossRef](#)]
28. McGilvray, K.L.; Fasciani, C.; Bueno-Alejo, C.J.; Schwartz-Narbonne, R.; Scaiano, J.C. Photochemical strategies for the seed-mediated growth of gold and gold–silver nanoparticles. *Langmuir* **2012**, *28*, 16148–16155. [[CrossRef](#)] [[PubMed](#)]
29. Czaplinska, J.; Sobczak, I.; Ziolk, M. Bimetallic AgCu/SBA-15 system: The effect of metal loading and treatment of catalyst on surface properties. *J. Phys. Chem. C* **2014**, *118*, 12796–12810. [[CrossRef](#)]
30. Fu, J.; Wang, S.; Zhu, J.; Wang, K.; Gao, M.; Wang, X.; Xu, Q. Au-Ag bimetallic nanoparticles decorated multi-amino cyclophosphazene hybrid microspheres as enhanced activity catalysts for the reduction of 4-nitrophenol. *Mater. Chem. Phys.* **2018**, *207*, 315–324. [[CrossRef](#)]
31. Hong, M.; Xu, L.; Wang, F.; Xu, S.; Li, H.; Li, C.Z.; Liu, J. In situ synthesized Au-Ag nanocages on graphene oxide nanosheets: A highly active and recyclable catalyst for the reduction of 4-nitrophenol. *New J. Chem.* **2016**, *40*, 1685–1692. [[CrossRef](#)]
32. Zhang, H.; Fei, C.; Zhang, D.; Tang, F. Degradation of 4-nitrophenol in aqueous medium by electro-Fenton method. *J. Hazard. Mater.* **2007**, *145*, 227–232. [[CrossRef](#)] [[PubMed](#)]
33. Zelekew, O.A.; Kuo, D.H. A two-oxide nanodiode system made of double-layered p-type Ag₂O@n-type TiO₂ for rapid reduction of 4-nitrophenol. *Phys. Chem. Chem. Phys.* **2016**, *18*, 4405–4414. [[CrossRef](#)] [[PubMed](#)]

34. Leishangthem, D.; Yumkhaibam, M.A.K.; Henam, P.S.; Nagarajan, S. An insight into the effect of composition for enhance catalytic performance of biogenic Au/Ag bimetallic nanoparticles. *J. Phys. Org. Chem.* **2018**, *31*, 3815. [[CrossRef](#)]
35. Al-Kahtani, A.A.; Almuqati, T.; Alhokbany, N.; Ahamad, T.; Naushad, M.; Alshehri, S.M. A clean approach for the reduction of hazardous 4-nitrophenol using gold nanoparticles decorated multiwalled carbon nanotubes. *J. Clean. Prod.* **2018**, *191*, 429–435. [[CrossRef](#)]
36. Kalantari, K.; Afifi, A.B.M.; Bayat, S.; Shameli, K.; Yousefi, S.; Mokhtar, N.; Kalantari, A. Heterogeneous catalysis in 4-nitrophenol degradation and antioxidant activities of silver nanoparticles embedded in Tapioca starch. *Arab. J. Chem.* **2017**. [[CrossRef](#)]
37. You, L.; Mao, Y.; Ge, J. Synthesis of stable SiO₂@Au-nanoring colloids as recyclable catalysts: Galvanic replacement taking place on the surface. *J. Phys. Chem. C* **2012**, *116*, 10753–10759. [[CrossRef](#)]
38. Yang, Y.; Shi, J.; Kawamura, G.; Nogami, M. Preparation of Au-Ag, Ag-Au core-shell bimetallic nanoparticles for surface-enhanced Raman scattering. *Scr. Mater.* **2008**, *58*, 862–865. [[CrossRef](#)]
39. Huang, J.; Li, Q.; Sun, D.; Lu, Y.; Su, Y.; Yang, X.; Wang, H.; Wang, Y.; Shao, W.; He, N.; et al. Biosynthesis of silver and gold nanoparticles by novel sun dried Cinnamomumcamphora leaf. *Nanotechnology* **2007**, *18*, 105104. [[CrossRef](#)]
40. Zhang, H.; Okuni, J.; Toshima, N. One-pot synthesis of Ag-Au bimetallic nanoparticles with Au shell and their high catalytic activity for aerobic glucose oxidation. *J. Colloid Interface Sci.* **2011**, *354*, 131–138. [[CrossRef](#)] [[PubMed](#)]
41. Ahmad, A.; Syed, F.; Shah, A.; Khan, Z.; Tahir, K.; Khan, A.U.; Yuan, Q. Silver and gold nanoparticles from *Sargentodoxa cuneata*: Synthesis, characterization and antileishmanial activity. *RSC Adv.* **2015**, *5*, 73793–73806. [[CrossRef](#)]
42. Krishnamurthy, S.; Esterle, A.; Sharma, N.C.; Sahi, S.V. Yucca-derived synthesis of gold nanomaterial and their catalytic potential. *Nanoscale Res. Lett.* **2014**, *9*, 627. [[CrossRef](#)] [[PubMed](#)]
43. Banerjee, M.; Sharma, S.; Chattopadhyay, A.; Ghosh, S.S. Enhanced antibacterial activity of bimetallic gold-silver core-shell nanoparticles at low silver concentration. *Nanoscale* **2011**, *3*, 5120–5125. [[CrossRef](#)] [[PubMed](#)]
44. Esparza, R.; Santoveña, A.; Ruíz-Baltazar, A.; Angeles-Pascual, A.; Bahena, D.; Maya-Cornejo, J.; Ledesma-García, J.; Pérez, R. Study of PtPd Bimetallic Nanoparticles for Fuel Cell Applications. *Mater. Res.* **2017**, *20*, 1193–1200. [[CrossRef](#)]
45. Tan, N.P.B.; Lee, C.H.; Li, P. Green synthesis of smart metal/polymer nanocomposite particles and their tuneable catalytic activities. *Polymers* **2016**, *8*, 105. [[CrossRef](#)]
46. Jana, N.R.; Gearheart, L.; Murphy, C.J. Seed-mediated growth approach for shape-controlled synthesis of spheroidal and rod-like gold nanoparticles using a surfactant template. *Adv. Mater.* **2001**, *13*, 1389. [[CrossRef](#)]
47. Yang, Y.; Matsubara, S.; Nogami, M.; Shi, J.; Huang, W. One-dimensional self-assembly of gold nanoparticles for tunable surface plasmon resonance properties. *Nanotechnology* **2006**, *17*, 2821. [[CrossRef](#)]
48. Dong, F.; Guo, W.; Park, S.K.; Ha, C.S. Controlled synthesis of novel cyanopropylpolysilsesquioxane hollow spheres loaded with highly dispersed Au nanoparticles for catalytic applications. *Chem. Commun.* **2012**, *48*, 1108–1110. [[CrossRef](#)] [[PubMed](#)]
49. Halder, K.K.; Kundu, S.; Patra, A. Core-size-dependent catalytic properties of bimetallic Au/Ag core-shell nanoparticles. *ACS Appl. Mater. Interfaces* **2014**, *6*, 21946–21953. [[CrossRef](#)] [[PubMed](#)]
50. Jono, R.; Tateyama, Y.; Yamashita, K. A method to calculate redox potentials relative to the normal hydrogen electrode in nonaqueous solution by using density functional theory-based molecular dynamics. *Phys. Chem. Chem. Phys.* **2015**, *17*, 27103–27108. [[CrossRef](#)] [[PubMed](#)]
51. Huo, S.; Ma, H.; Huang, K.; Liu, J.; Wei, T.; Jin, S.; Zhang, J.; He, S.; Liang, X.J. Superior penetration and retention behavior of 50 nm gold nanoparticles in tumors. *Cancer Res.* **2013**, *73*, 319–330. [[CrossRef](#)] [[PubMed](#)]
52. Xia, B.; He, F.; Li, L. Preparation of bimetallic nanoparticles using a facile green synthesis method and their application. *Langmuir* **2013**, *29*, 4901–4907. [[CrossRef](#)] [[PubMed](#)]
53. Zhang, L.; Xie, Z.; Gong, J. Shape-controlled synthesis of Au-Pd bimetallic nanocrystals for catalytic applications. *Chem. Soc. Rev.* **2016**, *45*, 3916–3934. [[CrossRef](#)] [[PubMed](#)]
54. Cao, S.; Tao, F.; Tang, Y.; Li, Y.; Yu, J. Size- and shape-dependent catalytic performances of oxidation and reduction reactions on nanocatalysts. *Chem. Soc. Rev.* **2016**, *45*, 4747–4765. [[CrossRef](#)] [[PubMed](#)]

55. Borhamdin, S.; Shamsuddin, M.; Alizadeh, A. Biostabilised icosahedral gold nanoparticles: Synthesis, cyclic voltammetric studies and catalytic activity towards 4-nitrophenol reduction. *J. Exp. Nanosci.* **2016**, *11*, 518–530. [[CrossRef](#)]
56. Wu, T.; Zhang, L.; Gao, J.; Liu, Y.; Gao, C.; Yan, J. Fabrication of graphene oxide decorated with Au-Ag alloy nanoparticles and its superior catalytic performance for the reduction of 4-nitrophenol. *J. Mater. Chem. A* **2013**, *1*, 7384–7390. [[CrossRef](#)]
57. Ko, F.H.; Chang, Y.C. Aptamer based surface enhanced Raman scattering detection of adenosine using various core sizes of Au-Ag core-shell nanoparticles. *RSC Adv.* **2014**, *4*, 26251–26257. [[CrossRef](#)]



© 2018 by the authors. Licensee MDPI, Basel, Switzerland. This article is an open access article distributed under the terms and conditions of the Creative Commons Attribution (CC BY) license (<http://creativecommons.org/licenses/by/4.0/>).